ORIGINAL RESEARCH

Targeted Delivery of Mesenchymal Stem Cell-Derived Bioinspired Exosome-Mimetic Nanovesicles with Platelet Membrane Fusion for Atherosclerotic Treatment

Yu Jiang [1],*, Miao Yu[1],*, Zhi-Feng Song[1],*, Zhi-Yao Wei[1], Ji Huang[2], Hai-Yan Qian [1]

[1]Center for Coronary Heart Disease, Department of Cardiology, Fu Wai Hospital, National Center for Cardiovascular Diseases of China, State Key Laboratory of Cardiovascular Disease, Chinese Academy of Medical Sciences and Peking Union Medical College, Beijing, People's Republic of China; [2]Center for Coronary Artery Disease, Division of Cardiology, Beijing Anzhen Hospital, Capital Medical University, Beijing Institute of Heart, Lung, and Blood Vessel Diseases, National Clinical Research Center for Cardiovascular Diseases, Beijing, People's Republic of China

*These authors contributed equally to this work

Correspondence: Ji Huang, Center for Coronary Artery Disease, Division of Cardiology, Beijing Anzhen Hospital, Capital Medical University, Beijing Institute of Heart, Lung, and Blood Vessel Diseases, National Clinical Research Center for Cardiovascular Diseases, Beijing, 100029, People's Republic of China, Email drjihuang@163.com; Hai-Yan Qian, Center for Coronary Heart Disease, Department of Cardiology, Fu Wai Hospital, National Center for Cardiovascular Diseases of China, State Key Laboratory of Cardiovascular Disease, Chinese Academy of Medical Sciences and Peking Union Medical College, 167 Beilishi Road, Beijing, 100037, People's Republic of China, Email ahqhy712@163.com

Purpose: Accumulating evidence indicates that mesenchymal stem cells (MSCs)-derived exosomes hold significant potential for the treatment of atherosclerosis. However, large-scale production and organ-specific targeting of exosomes are still challenges for further clinical applications. This study aims to explore the targeted efficiency and therapeutic potential of biomimetic platelet membrane-coated exosome-mimetic nanovesicles (P-ENVs) in atherosclerosis.

Methods: To produce exosome-mimetic nanovesicles (ENVs), MSCs were successively extruded through polycarbonate porous membranes. P-ENVs were engineered by fusing MSC-derived ENVs with platelet membranes and characterized using transmission electron microscopy (TEM), nanoparticle tracking analysis (NTA), and Western blot. The stability and safety of P-ENVs were also assessed. The targeted efficacy of P-ENVs was evaluated using an in vivo imaging system (IVIS) spectrum imaging system and immunofluorescence. Histological analyses, Oil Red O (ORO) staining, and Western blot were used to investigate the anti-atherosclerotic effectiveness of P-ENVs.

Results: Both ENVs and P-ENVs exhibited similar characteristics to exosomes. Subsequent miRNA sequencing of P-ENVs revealed their potential to mitigate atherosclerosis by influencing biological processes related to cholesterol metabolism. In an ApoE$^{-/-}$ mice model, the intravenous administration of P-ENVs exhibited enhanced targeting of atherosclerotic plaques, resulting in a significant reduction in lipid deposition and necrotic core area. Our in vitro experiments showed that P-ENVs promoted cholesterol efflux and reduced total cholesterol content in foam cells. Further analysis revealed that P-ENVs attenuated intracellular cholesterol accumulation by upregulating the expression of the critical cholesterol transporters ABCA1 and ABCG1.

Conclusion: This study highlighted the potential of P-ENVs as a novel nano-drug delivery platform for enhancing drug delivery efficiency while concurrently mitigating adverse reactions in atherosclerotic therapy.

Keywords: exosome-mimetic nanovesicles, platelet membrane-coated nanovesicles, biomimicry, targeted delivery, atherosclerosis

Introduction

Atherosclerosis is a chronic vascular disease characterized by the accumulation of lipid plaque within the arterial intima, gradually leading to arterial stenosis or occlusion.[1,2] As a hallmark of atherosclerotic lesions, foam cells play a pivotal role in the pathogenesis of atherosclerosis. Their aberrant lipid uptake, cholesterol esterification, and cholesterol efflux

precipitate the occurrence and progression of atherosclerosis.[3] Despite considerable progress in conventional treatments for atherosclerosis, there remains an imperative to develop more precise and effective therapeutic strategies. Recently, the rapid advancements in nanotechnology and biomedicine have brought nanoparticles as a promising direction for improving atherosclerotic treatment.[4] A primary objective of nanotherapy is to address the solubility problems of developed drugs, thus improving their therapeutic efficacy.[5,6] Currently, the principal nanoparticles being explored for atherosclerotic treatment include natural nanoparticles such as extracellular vesicles (EVs) nanoparticles, as well as synthetic nanoparticles such as polymer nanoparticles,[7–9] lipid nanoparticles,[10,11] and silicon nanoparticles.[12]

Engineering of synthetic nanoparticles allows for their precise customization in terms of size, shape, physical properties, and surface functionalities.[13] Capitalizing on their excellent biocompatibility and biodegradability, Pillai et al[7] developed an innovative polymer nanoparticle encapsulating a curcumin-BioPerine complex, which could enhance the anti-atherosclerotic efficacy of curcumin by reducing cholesterol levels in macrophages and curtailing foam cell formation. Moreover, several studies coated polymer nanoparticles with complex functional cell membranes,[14,15] which could attenuate macrophage phagocytosis and enhance the targeted delivery of these nanoparticles in atherosclerotic plaques.[16] Compared to metal nanoparticles[17,18] and silicon nanoparticles,[12] liposomes, composed of natural molecules, thus offer superior biocompatibility and a lower risk of adverse effects.[19] Gao et al[10] engineered a quercetin-loaded liposome that could be further conjugated with macrophages, forming a targeted macrophage-liposome complex for anti-atherosclerotic therapy, effectively alleviating inflammation, and facilitating cholesterol efflux. While synthetic nanoparticles present a high degree of customizability and potent therapeutic potential, their design and production processes are typically more complex and expensive than those of natural nanoparticles. Moreover, their in vivo safety and efficacy require further comprehensive studies.

Compared to synthetic nanoparticles, biological nanoparticles offer several advantages, including reduced toxicity, improved biocompatibility, and an enhanced ability to traverse biological barriers.[20,21] Previous studies have demonstrated that mesenchymal stem cells (MSCs)-derived exosomes, a classical type of EVs, have a significant therapeutic potential in atherosclerosis.[22–24] In contrast to MSC implantation, the administration of exosomes as a cell-free therapy for atherosclerotic treatment could mitigate the risks associated with immune reactions, tumorigenesis risk, and occlusions in distal microvasculature.[25] Owing to their enrichment of RNAs and proteins from parental MSCs,[26] the recent focus has transitioned from transplantation of MSCs to the application of their derived exosomes in atherosclerotic treatment.[27] Some studies have demonstrated that MSC-derived exosomes ameliorated abnormal cholesterol accumulation by modulating cholesterol influx and efflux in foam cells.[28,29] Besides, MSC-derived exosomes also reduced inflammation and exerted immunomodulatory effects, ultimately preventing the formation of unstable plaques.[30,31] Hence, an in-depth comprehension of MSC-derived exosomes will contribute to the development of innovative therapeutic approaches for atherosclerosis. Despite the therapeutic potential of MSC-derived exosomes, their clinical translation is limited by several challenges, such as the efficiency of production, the complexities of exosomal isolation and purification, and the precision of targeted delivery to recipient cells.[32–35]

To address these obstacles, recent studies have developed exosome-mimetic nanovesicles (ENVs) to mimic EVs by the serial extrusion of cells through microporous filters.[36–38] ENVs exhibit similar particle sizes, intracellular contents, and plasma membrane proteins as natural exosomes, and they can also transport biomolecules of their parental cells to recipient cells.[39,40] Furthermore, ENVs hold a 250-fold increase in production yield and a twofold greater abundance of RNA and proteins compared to exosomes derived from an equivalent number of cells.[41] Although ENVs have shown considerable promise in various fields, their potential in atherosclerotic treatment remains unexplored.[36–38,40,42–44] Collectively, ENVs emerge as a viable alternative to exosomes in terms of their higher production efficiency, cost-effectiveness, and therapeutic potency. Considering the potential off-target effects associated with the systemic administration of ENVs to atherosclerotic lesions, there has been a growing focus on the development of a targeted drug delivery system. Recent studies have revealed that a platelet-inspired targeted delivery system may provide innovative therapeutic platforms due to the natural targeted property of platelets for atherosclerotic plaques.[45–47] By utilizing the unique properties of platelets, platelet membrane-coated nanoparticles (P-NPs), a novel biomimetic material combining platelet membranes with nanoparticles, represent a potential to elevate biocompatibility, prolong circulation duration, and enhance targeted capability.[48–50] Consequently, the field of platelet membrane modification is emerging as a promising therapeutic platform for the targeted delivery of anti-atherosclerotic agents to plaques, enhancing therapeutic efficacy while reducing adverse side effects.

Here, platelet membrane-coated ENVs (P-ENVs) were developed as a biomimetic nanodrug delivery system by mimicking the natural adhesion of platelets to atherosclerotic lesions (Scheme 1). Briefly, we generated MSC-derived ENVs through a serial extrusion of MSCs using microporous filters. These ENVs were subsequently cloaked with platelet membranes, preserving almost all characteristics of both MSCs and platelet membranes. Both in vitro and in vivo studies were performed to assess the targeted ability and therapeutic effect of P-ENVs on atherosclerotic lesions.

Materials and Methods
Cell Culture
Mouse bone marrow MSCs (Procell Life Science & Technology, Wuhan, China) were cultured in Iscove's Modified Dulbecco's Medium (IMDM, Gibco, NY, USA) supplemented with 10% fetal bovine serum (FBS, Sigma–Aldrich, St. Louis, USA) and 1% penicillin–streptomycin (Gibco, NY, USA). MSCs from P3-P5 were used for all experiments.
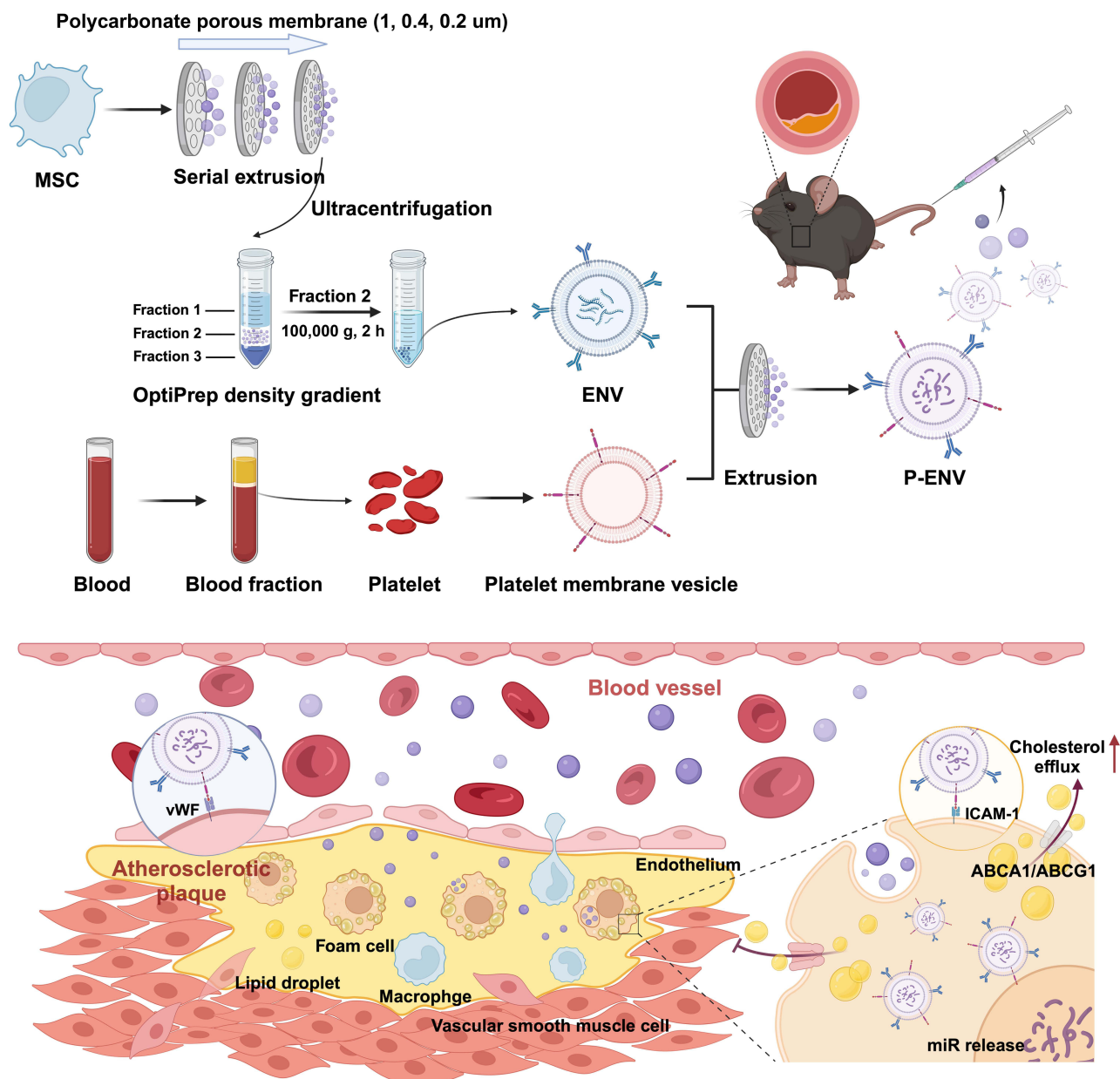
Scheme 1 Schematic illustration of targeted delivery of P-ENVs to plaques for atherosclerotic treatment.

Mouse aortic vascular smooth muscle cells (MVSMCs) and human aortic smooth muscle cells (HSMCs), both purchased from Procell Life Science & Technology (Wuhan, China), were cultured in Dulbecco's Modified Eagle Medium/Nutrient Mixture F-12 (DMEM/F-12, Sigma–Aldrich, St. Louis, USA). RAW264.7 cells (American Type Culture Collection, Virginia, USA) and human umbilical vein endothelial cells (HUVECs, American Type Culture Collection, Virginia, USA) were cultured in Dulbecco's Modified Eagle Medium (DMEM, Sigma–Aldrich, St. Louis, USA) and Endothelial Cell Medium (ECM, Sciencell, California, USA), respectively. All cell lines were maintained at 37 °C in a humidified environment containing 5% CO2.

Preparation of ENVs

To prepare ENVs, MSCs were resuspended in phosphate buffered saline (PBS, Servicebo, Wuhan, China) at 5×10^6 cells/mL and sequentially extruded 10 times each through 1um, 400 nm, and 200 nm polycarbonate porous membranes (Sigma–Aldrich, St. Louis, USA) in the Avanti mini extruder (Sigma–Aldrich, St. Louis, USA). The goal is to isolate ENVs from a mixture of cellular debris and free proteins. An iodixanol gradient solution (Axis-Shield, Dundee, UK) was performed, 50% iodixanol was placed at the bottom of an ultracentrifuge tube, overlaid with 10% iodixanol and the extruded samples, and then ultracentrifuged at $100,000 \times g$ for 2 h at 4 °C. ENVs were obtained from the interface of the 50% and 10% iodixanol layers and further pelleted at $100,000 \times g$ for 2 h at 4 °C.

Platelet Isolation and Platelet Membrane Extraction

All human experiments were performed in line with the Ethics Committee of Fuwai Hospital (FW-2020-1317) and followed the guidelines outlined in the Declaration of Helsinki. Besides, informed consent was obtained from the study participants.

Fresh human type O$^-$ blood was collected using dipotassium Ethylene Diamine Tetraacetic Acid (EDTA)-treated or lithium heparin-treated blood collection tubes to prevent platelet activation. To isolate platelet-rich plasma (PRP), the whole blood was centrifuged at $100 \times g$ for 20 min at room temperature to extract the supernatant PRP. The resulting PRP was then centrifuged again at $100 \times g$ for 20 min to separate red blood cells and white blood cells. Platelets were resuspended in PBS containing 1mM EDTA (Solarbio, Beijing, China) and 2 mM prostaglandin E1 (PGE1, Sigma-Aldrich, St. Louis, USA) to prevent platelet activation. Platelet membranes were derived by a repeated freeze–thaw process and pelleted by centrifugation at $4000 \times g$ for 3 min. Then platelet membranes were suspended and sonicated in a capped glass vial for 5 min using an Ultrasonic Cell Crusher VCX130 (Sonics, Connecticut, USA) at a frequency of 42 kHz and a power of 100 W. Finally, they were extruded sequentially through 400 nm and 200 nm polycarbonate porous membranes 10 times each in the Avanti mini extruder.

Preparation and Characterization of P-ENVs

ENVs and platelet membrane vesicles were mixed at an equal protein ratio in the presence of 5% polyethylene glycol (PEG, Solarbio, Beijing, China). To modify the platelet membranes onto the surface of ENVs, the mixture was extruded 10 times through 400 nm and 200 nm polycarbonate porous membranes, respectively. The size distribution and morphology of ENVs and P-ENVs were measured by nanoparticle tracking analysis (NTA) and transmission electron microscopy (TEM), respectively. To identify the surface markers of platelet membrane vesicles, ENVs, and P-ENVs, Western blot analysis was used. The stability of ENVs and P-ENVs was assessed following incubation with PBS and 10% FBS at 37°C. Then, particle size measurements were conducted at different time points using NTA.

Evaluation of Cellular Viability

According to the CCK-8 assay protocol (Beyotime, Shanghai, China), cells were planted at a density of 1×10^4 cells/mL into a 96-well plate, with each well containing 100 μL of the cell suspension. After cell attachment, the corresponding treatments were administered for a duration of 24 h. Then, 10 μL of CCK-8 solution was added into each well, followed by incubation at 37°C for 2 h. The optical density (OD) was then measured at 450 nm wavelength.

Total RNA Isolation and miRNA Sequencing

Total RNA was extracted from ENVs and P-ENVs using the RNeasy Mini Kit (Qiagen, Dusseldorf, Germany) according to the manufacturer's protocol. Following the extraction process, the concentration of total RNA and the A260:A280 ratio were assessed utilizing the NanoDrop 2000 spectrophotometer (Thermo Fisher Scientific, Massachusetts, USA). Then, the total RNA was employed in the construction of a next-generation sequencing library according to the protocol of TruSeq RNA Library Preparation Kit V2 (Illumina, San Diego, USA). The cDNA products underwent amplification, and sequencing adapters along with barcodes were ligated onto fragments from each sample to create cDNA libraries ready for sequencing. The sequencing was performed by Biotechnology Corporation (Shanghai, China), using the HiSeq X Ten platform (Illumina, San Diego, USA). The differential expression of miRNAs between the ENV and P-ENV groups was analyzed using the independent sample t-test, with a significance threshold of 0.05. Subsequently, the target genes associated with these miRNAs were identified using the "Starbase" database. Gene Ontology (GO) and Kyoto Encyclopedia of Genes and Genomes (KEGG) analyses were performed using the "KOBAS" database.

Endothelial Targeting Ability

HUVECs were pre-stimulated with 100 ng/mL lipopolysaccharide (LPS, Sigma–Aldrich, St. Louis, USA) for 24 h to upregulate von Willebrand Factor (vWF) expression. Then HUVECs were incubated with DiI-labelled ENVs or P-ENVs. After 30 min of incubation, the cells were washed three times and stained with anti-vWF antibody. The fluorescent intensity of these samples was subsequently measured by laser confocal microscopy (Leica SP8, Hessian, German).

P-ENV Uptake by Foam Cells

For foam cell conversion, vascular smooth muscle cells (VSMCs) were cultured for 24 h in the presence of ox-LDL (Yiyuan Biotech, Guangzhou, China; 80 μg/mL). DiI-labelled ENVs or P-ENVs was then added and cultured for 4 h. Then, cells were washed with PBS three times and stained with phalloidin (Abcam, Cambridge, UK). The internalization of DiI-labelled ENVs or P-ENVs was subsequently assessed under laser confocal microscopy.

ORO Staining

VSMCs were stimulated with 80 μg/mL ox-LDL before in combination with ENVs or P-ENVs for 24 h. Next, VSMCs were fixed in 4% paraformaldehyde for 15 min and rinsed with PBS three times. The cells were then stained with Oil Red O (ORO, Sigma-Aldrich, St. Louis, USA) for 30 min at room temperature. ORO staining was imaged by optical microscopy (Olympus, Tokyo, Japan) and quantified by Image J software.

DIL-oxLDL Uptake Assay

VSMCs were pretreated with ox-LDL (80 μg/mL) for 24 h and then incubated with ENVs or P-ENVs for another 24 h. 10 μg/mL Dioctadecyl 3,3,3,3-tetramethylin docarbocyanine-oxLDL (DIL-oxLDL, Yiyuan Biotech, Guangzhou, China) was added into medium for 4 h and then washed with PBS. The uptake of DIL-oxLDL by VSMCs was observed under laser confocal microscopy.

Total Cholesterol Content Assay

Intracellular total cholesterol content was measured by the cholesterol fluorometric assay kit (Cayman Chemical, Michigan, USA) according to the manufacturer's instruction. VSMCs were washed with PBS and lysed with 0.5% Triton X-100. The mixture was then taken out and centrifuged at $18,000 \times$ g at 4°C for 30 min. The supernatants were used for cholesterol measurements. A standard curve of cholesterol reference was used to calculate intracellular cholesterol levels after normalization with protein.

Cholesterol Efflux Assay

VSMCs were incubated with ENVs or P-ENVs for 24 h and then incubated with 10 μmol/L Nitrobenzoxadiazolyl (NBD)-cholesterol (Cayman Chemical, Michigan, USA) for 4 h. After cholesterol loading, the NBD-cholesterol labeled

VSMCs were washed with PBS twice and then incubated with apolipoprotein A-I (APOA-I, Sigma-Aldrich, St. Louis, USA; 15 μg/mL) for 4 h. The fluorescence-labeled cholesterol was released from VSMCs into the medium, and VSMCs were lysed at 37°C with 0.3 M NaOH solution for 15 min. The fluorescence intensity (FI) of the medium and lysate was measured at 472 nm excitation and 540 nm emission light using a microplate spectrophotometer. The efflux rate was calculated using the following equation: Efflux (%) = FI (efflux medium): [FI (efflux medium) + FI (cell lysate)] × 100.

Targeting Atherosclerotic Plaques of P-ENVs in vivo

To track P-ENVs in vivo, we labeled ENVs and P-ENVs with DiD. Then, ApoE$^{-/-}$ mice with atherosclerotic plaque were randomized into three groups to receive PBS, DiD-labelled ENVs, and DiD-labelled P-ENVs through the tail vein. The mice in each group were euthanized at 0.5, 2, and 6 h, respectively. Arterial trees and other major organs (heart, liver, lung, spleen, brain, and kidney) were isolated. An in vivo imaging system (IVIS) spectrum imaging system (PerkinElmer, Massachusetts, USA) was performed to analyze the distribution of the fluorescent intensity in different organs.

Treatment Protocol for Atherosclerotic Mice

The animal experiment was conducted under the approval and supervision of the Experimental Animals Ethics Committee of Fuwai Hospital (FW-2022-0027), and all procedures met the National Institutes of Health guidelines.

ApoE$^{-/-}$ mice after 12 weeks of a western-type diet (Research diets, D12108C, 40 kcal% fat, and 1.25% cholesterol) were randomized into 3 groups (6 mice per group) and subjected to different treatments twice a week via tail vein for an additional 1 month. In treatment groups, mice were treated with ENVs or P-ENVs at a dose of 150 ug of ENVs, while mice were injected with only the same volume of PBS served as the control group.

Histological Study of Aortic Roots

For quantitative analysis of atherosclerotic plaques, the frozen sections (10 μm thick) were stained with ORO and hematoxylin–eosin (HE). Sections of the main organs including the heart, liver, lung, spleen, brain, and kidney were also analyzed by HE staining to evaluate the biosafety of P-ENVs.

Quantitative Analysis of the Atherosclerotic Plaques

After 4 weeks of treatment, the mice were sacrificed under anesthesia. Pathological evolution was evaluated by measuring the atherosclerotic plaque lesions in the aorta from the aortic root to the iliac bifurcation. Briefly, each aorta was carefully dissected and periadventitial tissue was cleaned. After the aorta was opened longitudinally, the entire aorta was stained with ORO to quantify the atherosclerotic plaque area.

Statistical Analysis

All data were reported as the mean ± standard deviation (SD) in this study. Statistical analysis was performed using GraphPad Prism 9. Student's *t*-test or one-way ANOVA was used for statistical analysis. The difference in significance level was set to *$p < 0.05$, **$p < 0.01$, and ***$p < 0.001$.

Results

Production and Characterization of ENVs and P-ENVs

To obtain ENVs, the MSCs, characterized by high expression of CD44 (Figure S1), were isolated from mouse bone marrow and serially extruded through polycarbonate porous membranes with pore sizes of 1 μm, 400 nm, and 200 nm. Then we engineered a platelet-mimicking targeted delivery platform (P-ENVs) through the extrusion of natural platelet membranes and ENVs. Compared with exosomes, the TEM revealed that most ENVs and P-ENVs were well-closed vesicles and P-ENVs were coated with platelet membranes (Figure 1A). The NTA analysis of ENVs and P-ENVs revealed a size distribution with peak diameters of approximately 142.5 nm and 150.9 nm, respectively, which were comparable to that of exosomes (130.9 nm) (Figure 1B). The successful fusion of platelet membranes and ENVs was further determined by fluorescence microscopy. We labeled ENVs with DiI membrane dye and labeled platelet
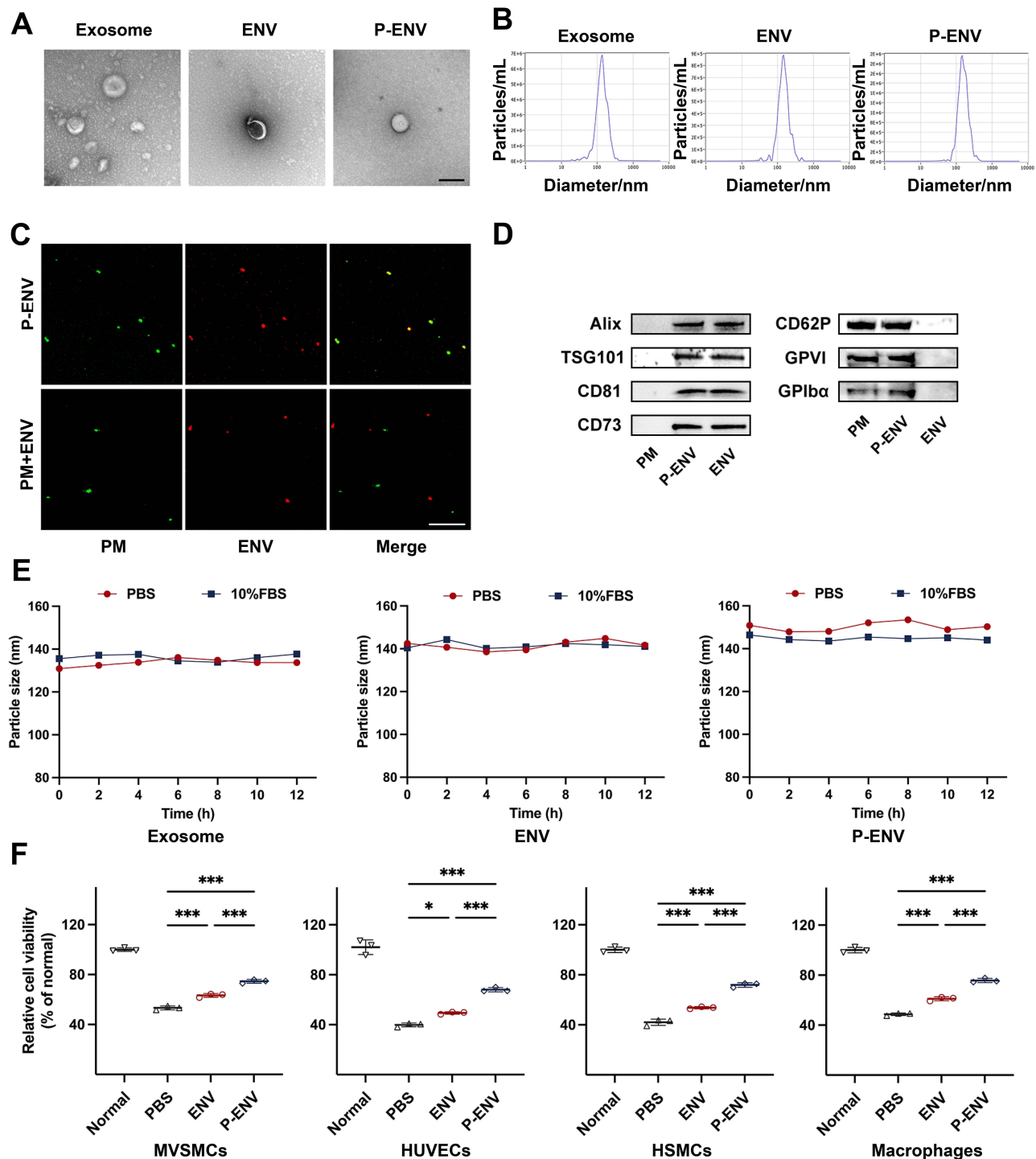
Figure 1 Fabrication and characterization of P-ENV. (**A**) Representative TEM images of exosome, ENV and P-ENV. Scale bar = 200 nm. (**B**) Size distribution of exosome, ENV and P-ENV by NTA analysis. (**C**) Colocalization analysis of P-ENV (yellow) or a simple mixture of PM (green) and ENV (red) by confocal fluorescence images. Scale bar = 20 um. (**D**) Western blot analysis of Alix, TSG101, CD81 and CD73 expression or CD62P, GPVI and GPIbα expression in platelet membrane (PM), ENV and P-ENV. (**E**) The particle sizes of exosome, ENV and P-ENV after incubation with PBS or serum. (**F**) Relative cell viability as evaluated by CCK-8 assay after various treatments. n = 3. All data are presented as mean ± SD (*$P < 0.05$, ***$P < 0.001$).

membranes with DiO membrane dye to observe the colocalization relationship, only the P-ENV group showed good colocalization, and the merged signal for platelet membranes and ENVs were represented by yellow fluorescence (Figure 1C). Western blot analysis indicated that both ENVs and P-ENVs contained exosome-specific markers including CD81, TSG101, and Alix, and the important platelet-specific markers (GPVI, GPIbα, and CD62P) were exclusively

presented on P-ENVs. In addition, ENVs and P-ENVs also expressed MSC specific surface marker CD73 (Figure 1D). The stability analysis of exosomes, ENVs, and P-ENVs demonstrated that there were no significant changes in particle size when incubated in PBS and 10% serum for 12 h (Figure 1E). Taken together, these results indicated that P-ENVs exhibited similarities with exosomes and presented an effective membrane fusion effect. In addition, to evaluate whether P-ENVs affect cell viability after cellular uptake, a CCK-8 cell viability assay was performed on MVSMCs, HUVECs, HSMCs, and macrophages under atherosclerotic conditions induced by ox-LDL. As depicted in Figure 1F, the cell viability was decreased after treatment with ox-LDL, but this ox-LDL-induced cytotoxicity was mitigated after the administration of P-ENVs (P < 0.001).

miRNA Expression in P-ENVs

Emerging evidence has demonstrated that exosomal miRNAs are key regulators of cellular functions.[26] To ascertain the critical role of miRNAs within ENVs in regulating foam cell formation and to further evaluate the integrity of the contents of P-ENVs, we performed a small RNA sequencing analysis on both ENVs and P-ENVs. As illustrated in Figure 2A, no statistically significant differences were observed in total miRNA profiles between ENVs and P-ENVs. Heatmap analysis also showed a similarity in miRNA expression between ENVs and P-ENVs, particularly in the top 10 significantly expressed miRNAs (Figure 2B). Based on GO and KEGG analysis, we identified the target genes associated with the miRNAs and explored the pathways and functions in which they were enriched. As shown in Figure 2C, the target gene numbers and rich factors related to the biological process of foam cell formation exhibited striking similarities between the ENV and P-ENV groups. Furthermore, both ENV and P-ENV groups demonstrated no significant difference in terms of cellular components, molecular functions, and the cholesterol metabolism signal pathway (Figure 2C and D). Next, to better understand the connection between miRNAs and their target genes in cholesterol metabolism signal pathway, we utilized Cytoscape for the analysis of miRNA-target gene interaction (Figure 2E). Collectively, our research illustrated the potential of bioinspired ENVs to alleviate the progression of atherosclerosis via modulating biological processes associated with foam cell formation. Moreover, the modification of platelet membrane did not yield a significant difference in miRNA profiles when compared with unmodified ENVs.

Targeting Effect and Cellular Uptake of P-ENVs

To evaluate whether P-ENVs had a superior targeted ability to atherosclerotic plaques in vivo, the ENVs and P-ENVs were labeled with DiD and intravenously injected into atherosclerotic mice. After 0.5 h, 2 h, and 6 h post injection, the IVIS images observed that P-ENVs were more prone to accumulate in atherosclerotic aortas compared with ENVs (P < 0.05 in 0.5 h; P < 0.001 in 2, 6 h). By contrast, the biodistribution of ENVs and P-ENVs was similar in other major organs (heart, liver, lung, spleen, brain, and kidney) (Figure 3A and B). Consistent with this result, fluorescence intensity in frozen sections of aorta roots was observed using a confocal microscope. The higher fluorescence intensity in P-ENV group exhibited a stronger targeted ability of P-ENVs to atherosclerotic plaques compared with ENVs (Figure S2). Although P-ENVs presented an enhanced targeted ability towards atherosclerotic plaques, their biodistribution was constrained by the widespread reticuloendothelial system (RES) within organs such as the liver and spleen.[34,51] A higher fluorescence intensity indicates a more extensive accumulation of ENVs and P-ENVs in these RES organs (Figure 3A and B). Then we assessed the targeted ability of P-ENVs to the injured endothelium in vitro, HUVECs were stimulated by LPS (100 ng/mL) for 24 h to express vWF on membranes and then incubated with DiI-labelled ENVs or P-ENVs for 30 min. As shown in Figure 3C and D, the P-ENV group exhibited higher red fluorescence signals on cell surfaces than ENV group (P-ENVs 368.6 ± 113.9 versus ENVs 125.3 ± 19.2; P < 0.001). We further evaluated the cellular uptake efficiency of P-ENVs by foam cells in vitro, mouse VSMCs were converted to foam cells by 80 μg/mL ox-LDL treatment. It was observed that the expression of intracellular adhesion molecule-1 (ICAM-1) by foam cells increased significantly (P < 0.001) (Figure S3), which mediated platelet and foam cell adhesion by interacting with platelet αIIbβ3. Then foam cells were incubated with DiI-labeled ENVs or P-ENVs for another 4 h, compared with ENVs, P-ENVs were abundantly observed in the cytoplasm of foam cells (P < 0.01) (Figure 3E and F), indicating that P-ENVs retained multiple adhesive functions of platelets and enhanced cellular uptake by foam cells.
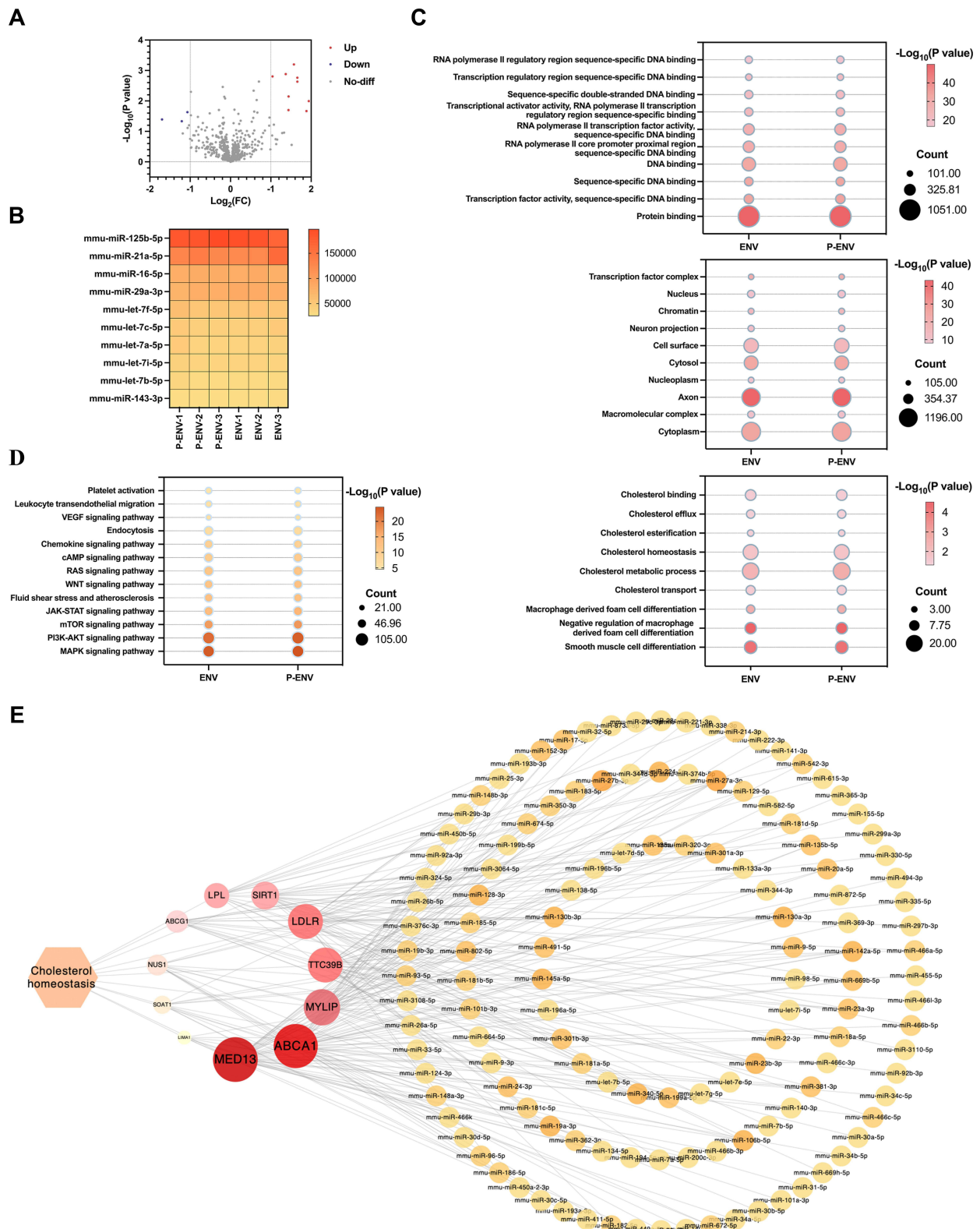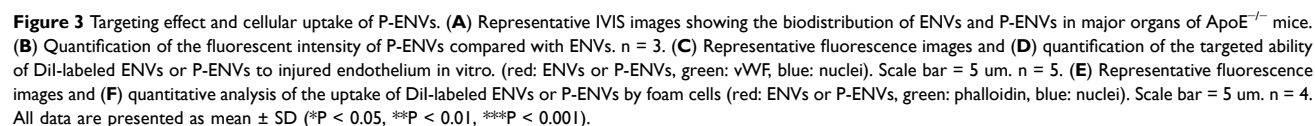
Figure 2 miRNA expression in P-ENVs. (**A**) Volcano plot of different miRNAs between ENV and P-ENV group. (**B**) Heatmap analysis of the top 10 expressed miRNAs between ENV and P-ENV group. (**C**) GO enrichment analysis for BP, CC, and MF on common genes identified in ENV and P-ENV group. (**D**) KEGG pathway analysis on genes related to cholesterol metabolism pathway in ENV and P-ENV group. (**E**) Cytoscape analysis on the interaction between miRNAs and target genes in cholesterol metabolism pathway. n = 3.

Figure 3 Targeting effect and cellular uptake of P-ENVs. (**A**) Representative IVIS images showing the biodistribution of ENVs and P-ENVs in major organs of ApoE$^{-/-}$ mice. (**B**) Quantification of the fluorescent intensity of P-ENVs compared with ENVs. n = 3. (**C**) Representative fluorescence images and (**D**) quantification of the targeted ability of DiI-labeled ENVs or P-ENVs to injured endothelium in vitro. (red: ENVs or P-ENVs, green: vWF, blue: nuclei). Scale bar = 5 um. n = 5. (**E**) Representative fluorescence images and (**F**) quantitative analysis of the uptake of DiI-labeled ENVs or P-ENVs by foam cells (red: ENVs or P-ENVs, green: phalloidin, blue: nuclei). Scale bar = 5 um. n = 4. All data are presented as mean ± SD (*P < 0.05, **P < 0.01, ***P < 0.001).

In vitro Anti-Atherosclerotic Efficacy of P-ENVs

To explore the potential of P-ENVs in regulating VSMC-derived foam cell formation in vitro, we treated ox-LDL-stimulated VSMCs with ENVs or P-ENVs. As shown in Figure 4A and B, compared with ENV group (P < 0.05) and control group (P < 0.001), P-ENV group showed remarkably decreased cellular lipid accumulation by ORO staining. We further detected the total cholesterol content in each group. As expected, the P-ENV group induced lower levels of total cholesterol content, compared with ENV group (P < 0.01) and control group (P < 0.001) (Figure 4C). Given that
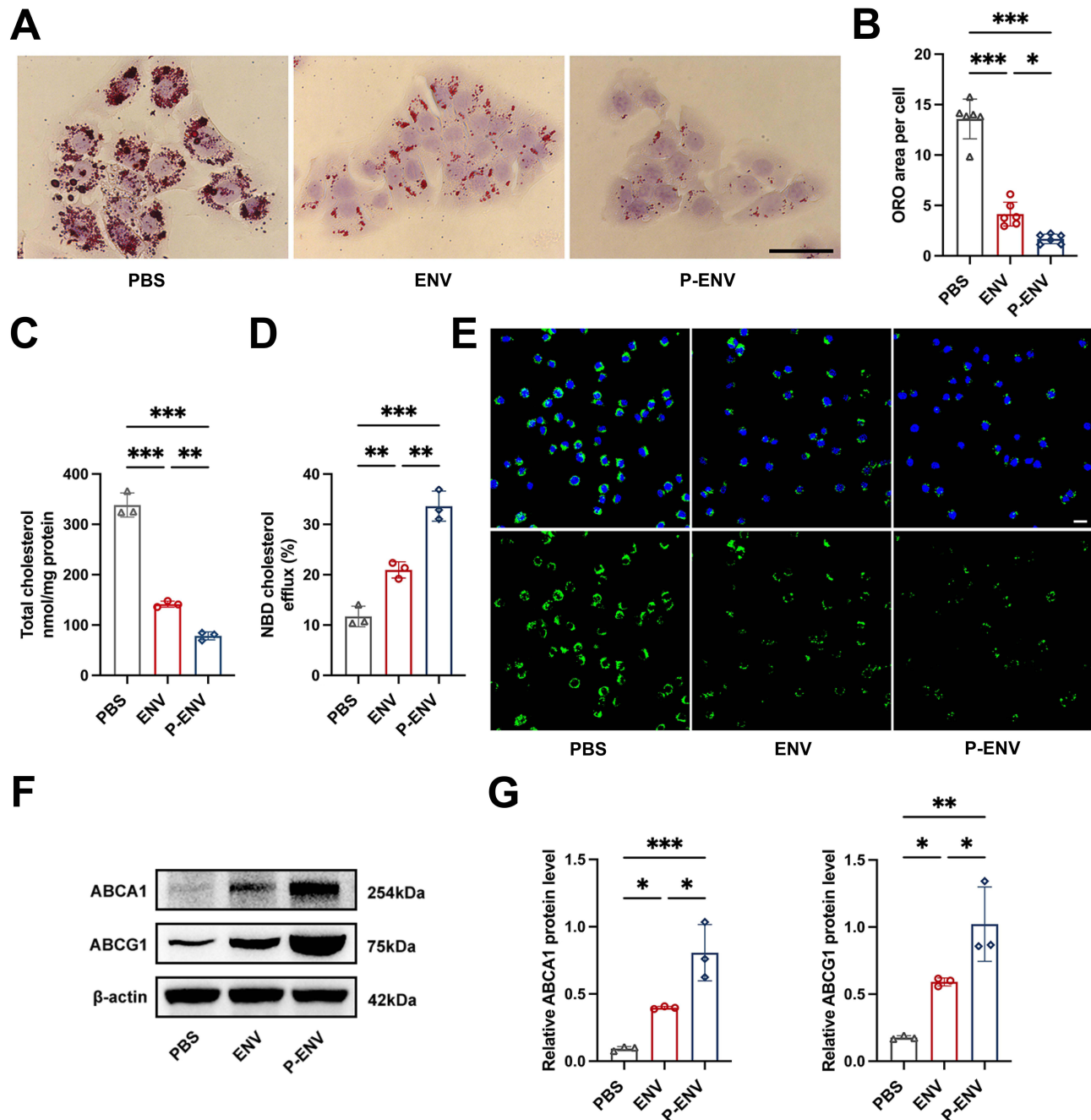
Figure 4 In vitro anti-atherosclerotic efficacy of P-ENVs. (**A**) Representative ORO images of ox-LDL-loaded VSMCs and (**B**) quantitative analysis of ORO area after treatment with PBS, ENVs, or P-ENVs in vitro. Scale bar = 50 um. n = 6. (**C**) Total cholesterol levels in foam cells after treatment with PBS, ENVs, or P-ENVs in vitro. n = 3. (**D**) Quantitative analysis of APOA-I mediated cholesterol efflux (%) in control, ENV, or P-ENV group and (**E**) representative fluorescent images of the NBD-cholesterol accumulation in foam cells obtained from these groups after incubation with APOA-I for 4 h. (green: NBD-cholesterol, blue: nuclei). Scale bar = 20 um. n = 3. (**F**) Western blot analysis and (**G**) quantification of ABCA1 and ABCG1 after various treatments in vitro. n = 3. All data are presented as mean ± SD (*P < 0.05, **P < 0.01, ***P < 0.001).

alterations in lipid uptake may affect lipid accumulation in foam cells, VSMCs were pretreated with ox-LDL and subsequently incubated with ENVs or P-ENVs prior to incubation with DIL-oxLDL. As depicted in Figure S4, our confocal microscopy analysis found that compared with control group, the phagocytosis of DIL-oxLDL was not affected by ENVs or P-ENVs. Next, NBD-cholesterol was used to evaluate whether P-ENVs could modulate cholesterol efflux. Compared with ENV group ($P < 0.01$) and control group ($P < 0.001$), treatment with P-ENVs significantly promoted cholesterol efflux to APOA-I (Figure 4D and E). We also analyzed the expression of cholesterol transporter-related protein ABCA1 and ABCG1. Consistent with these results, significantly higher ABCA1 and ABCG1 protein levels were detected in P-ENV group compared with ENV group ($P < 0.05$) and control group ($P < 0.01$) (Figure 4F and G). Given their pivotal role in reverse cholesterol transport (RCT), the upregulation of both ABCA1 and ABCG1 could accelerate the intracellular cholesterol efflux. Overall, these results indicated that P-ENVs might inhibit VSMC-derived foam cell formation via promoting cholesterol efflux.

In vivo Anti-Atherosclerotic Therapy of P-ENVs

To assess the anti-atherosclerotic effect of P-ENV treatment in atherosclerotic progression, we administered PBS, ENVs, or P-ENVs to ApoE$^{-/-}$ mice for 4 weeks (Figure 5A). As shown in Figure 5B and C, P-ENVs exhibited the strongest anti-atherosclerotic effects with the smallest plaque area ($8.3 \pm 0.9\%$) which was lower than ENV group ($15.9 \pm 1.0\%$, $P < 0.001$) and control group ($29.6 \pm 3.5\%$, $P < 0.001$). Consistent with these findings, ORO-stained cross-sections of aortic roots in P-ENV group exhibited reduced lipid deposition and the smallest lesion area, in comparison with ENV group ($P < 0.001$) and control group ($P < 0.001$) (Figure 5D and E). As shown by HE staining, treatment with P-ENVs significantly reduced the necrotic core area ($6.7 \pm 1.0\%$), compared with ENV group ($13.5 \pm 2.2\%$, $P < 0.01$) and control group ($28.2 \pm 3.4\%$, $P < 0.001$) (Figure 5D and F). To further determine the impact of P-ENVs on the expression of ABCA1 and ABCG1 in vivo, we assessed the level of ABCA1 and ABCG1 receptors in aortic tissues with plaques. Our Western blotting analysis revealed a marked upregulation of ABCA1 and ABCG1 in P-ENV group, compared with ENV group ($P < 0.05$) and control group ($P < 0.01$) (Figure 5G and H). Collectively, these findings indicated that P-ENVs exerted a strong anti-atherosclerotic effect, probably attributable to their targeted delivery.

Biosafety of P-ENVs in ApoE$^{-/-}$ Mice

The efficacy and safety of P-ENVs were assessed after a four-week treatment, and then the blood and major organs were collected for analysis. As shown in Figure 6A, lipid profiles in ApoE$^{-/-}$ mouse models were evaluated after P-ENV treatment. The levels of serum lipids, including triglyceride (TG), total cholesterol (TC), low-density lipoprotein (LDL), and high-density lipoprotein (HDL), were not obviously influenced by ENV or P-ENV treatment. Consistent with previous studies on targeted drug delivery for atherosclerotic treatment,[47,52] no difference in serum lipid profiles after treatment indicated that P-ENVs exerted targeted anti-atherosclerotic effects on the lesioned arteries, without altering serum lipid levels to achieve their therapeutic effects. Besides, the mounts of red blood cells (RBCs), white blood cells (WBCs), platelets (PLTs), and hemoglobin (HGB) in ENV and P-ENV groups were comparable to those observed in control group (Figure 6B). The hepatic and renal functions after exposure to ENVs and P-ENVs showed no distinguishable differences in creatinine (CREA), blood urea nitrogen (BUN), alanine aminotransferase (ALT), and aspartate aminotransferase (AST) (Figure 6C). Furthermore, as revealed in HE staining, no significant histopathological differences were observed in either ENV or P-ENV group compared with PBS group, indicating that ENVs and P-ENVs caused no remarkable toxicity or injury to major organs (Figure 6D). These results suggested that P-ENVs were safe and biocompatible candidates for long-term treatment, with no adverse effects observed in vivo.

Discussion

In this study, we developed P-ENVs as a targeted delivery system for anti-atherosclerotic treatment. Our results indicated that (i) MSCs-derived ENVs were successfully produced, exhibiting similarities to exosomes; (ii) P-ENVs were subsequently yielded by fusing ENVs with platelet membranes; (iii) P-ENVs showed superior targeted and specific accumulation in atherosclerotic plaques both in vitro and in vivo; (iv) P-ENVs were efficiently internalized by foam cells, leading to a decrease in intracellular lipid accumulation by promoting cholesterol efflux; (v) In an ApoE$^{-/-}$ mice model,
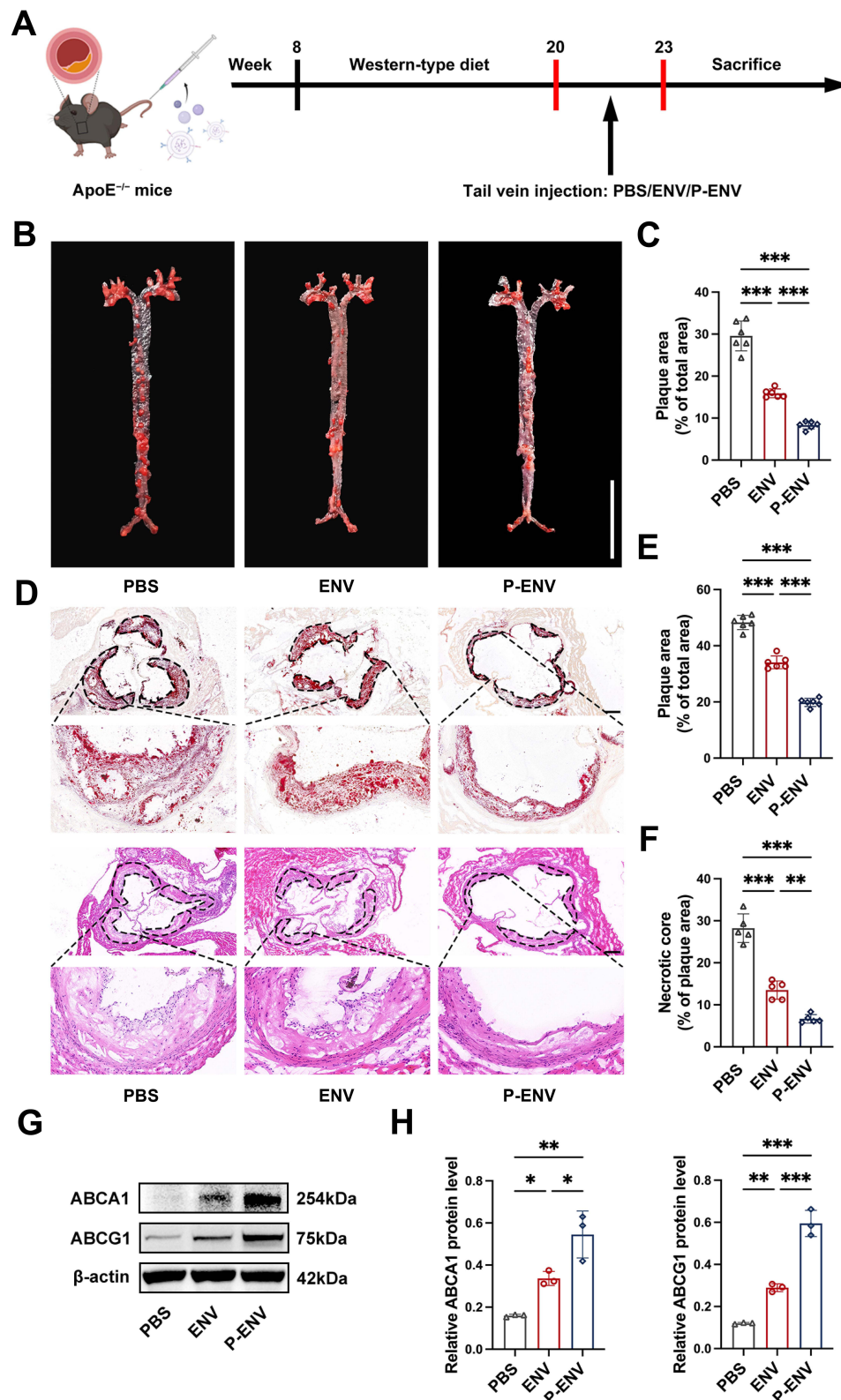
Figure 5 In vivo anti-atherosclerotic efficacy of P-ENVs. (**A**) Schematic diagram of the 4-week treatment of P-ENVs in ApoE$^{-/-}$ mice. (**B**) Representative images of en face ORO-stained aortas after treatment with PBS, ENVs, or P-ENVs in vivo. Scale bar = 10 mm. n = 6. (**C**) Quantification of plaque area in aortas. (**D**) Representative ORO and H&E images of aortic roots and quantitative analysis on (**E**) plaque area and (**F**) necrotic core after treatment with PBS, ENVs, or P-ENVs. Scale bar = 200 um. n = 5 or 6. (**G**) Western blot analysis and (**H**) quantification of ABCA1 and ABCG1 after 4-week treatment with PBS, ENVs, or P-ENVs in vivo. n = 3. All data are presented as mean ± SD (*P < 0.05, **P < 0.01, ***P < 0.001).
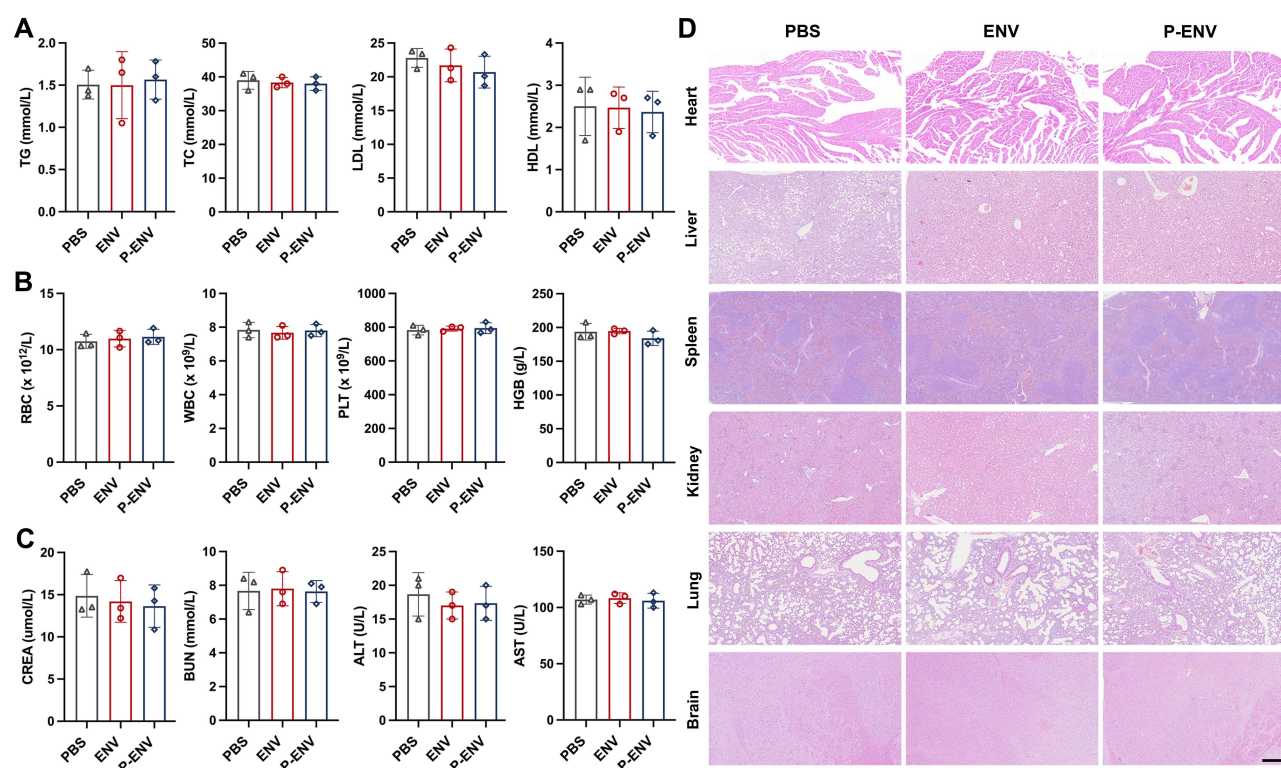
Figure 6 Biosafety of P-ENVs in ApoE$^{-/-}$ mice. (**A**) Quantification of TG, TC, LDL, and HDL after 4-week treatment with PBS, ENVs, or P-ENVs. n = 3. (**B**) Quantification of RBCs, WBCs, PLTs, and HGB after 4-week various treatments. n =3. (**C**) Quantification of CREA, BUN, ALT, and AST in various treatment groups. n = 3. (**D**) Representative H&E staining of heart, liver, spleen, kidney, lung, and brain of ApoE$^{-/-}$ mice treated with PBS, ENVs, or P-ENVs in vivo. Scale bar = 400 um. All data are presented as mean ± SD.

intravenous injection of P-ENVs resulted in an anti-atherosclerotic effect, characterized by reduced lipid deposition and a smaller necrotic core area.

Recently, P-NPs have emerged as an increasingly popular biomimetic platform. Due to their remarkable ability to mimic the surface characteristics of platelet membranes, a highly specific top-down approach has been applied in several diseases, including cardiovascular diseases,[53,54] cancers,[55,56] traumas,[57] and immune thrombocytopenia purpura.[58] It has been known that platelets play a pivotal role throughout the different stages of atherosclerotic progression.[59] Even at the onset of atherosclerosis, there is a significant interaction between platelets and injured endothelial cells, mediated by shear-dependent binding to vWF.[60,61] Furthermore, platelets exhibit strong adhesion to subendothelial collagen, which promotes the aggregation of activated platelets and leads to the formation of potentially life-threatening thrombi.[62] Given the inherent characteristics of platelets to target atherosclerotic plaques, in previous studies, the platelet-mimicking adhesive property of P-NPs was initially assessed via evaluating their binding efficiency to human type IV collagen and fibrin in vitro.[47] The P-NPs exhibited markedly improved retention in both collagen-binding test and fibrin-binding test, compared with uncoated nanoparticles. In our study, we further proved the platelet-mimicking adhesive functionality of P-ENVs to injured endothelium. In addition to confirming the adhesive property of P-ENVs in vitro, we also evaluated their targeted ability towards atherosclerotic lesions in vivo. The whole biodistribution analysis via IVIS images demonstrated a greater propensity of P-ENVs to accumulate in atherosclerotic aortas compared with unmodified ENVs, with no noticeable difference observed in other major organs. In line with this result, confocal image of aortic roots revealed that P-ENVs exhibited a remarkable capacity to accumulate at atherosclerotic plaques. Compared to the traditional approach of mimicking a single targeted ligand on platelet membrane surfaces, P-NPs possessed the complete surface properties of platelets, which enabled them to interact with multiple targets simultaneously and participate in intricate multicellular interactions in atherosclerotic lesions. Their exceptional biocompatibility and stability contributed to the inhibition of immunological rejection and provided protection for internal nanoparticles against degradation or clearance. Furthermore, the enhanced targeting ability of P-NPs facilitated the

precise delivery of drugs or nanoparticles to specific cells or tissues.[36,42,45–47] In our study, we observed a significant increase in ICAM-1 expression on foam cells following exposure to ox-LDL stimulation. This upregulation, in turn, mediated platelet adhesion through interaction with platelet αIIbβ3.[63,64] Under the context of this interaction, we observed an increased fluorescence intensity in foam cells following incubation with DiI-labelled P-ENVs. These findings served as compelling evidence that platelet membrane fusion substantially enhanced the uptake efficiency of foam cells. In conclusion, P-NPs emerge as a promising strategy for enhancing the efficiency of drug or nanoparticle delivery while concurrently mitigating potential adverse reactions.

Recent studies have focused on the development of artificial nanovesicles (ENVs) as an alternative to exosomes.[36–38,40,42–44] In concordance with these studies, we presented compelling evidence that MSCs-derived ENVs maintained their spherical shapes, demonstrated high stability, and exhibited a comparable range to those of MSC-derived exosomes through a serial extrusion process with polycarbonate porous membranes. Moreover, ENVs demonstrated a superior production yield and a higher content of proteins and miRNAs compared to traditional exosomes, emerging as promising substitutes for exosomes for clinical applications.[41] Based on the exosome-like characteristics of ENVs, a recent study revealed that neural progenitor cell-derived ENVs were found to significantly enhance the proliferation of dermal papilla cells (DPCs) and accelerate the transition of hair follicle cycling in a mouse model of depilation-induced hair regeneration.[37] Additionally, ENVs derived from a murine pancreatic β-cell line successfully solved the challenge of sourcing functional islets for transplantation and induced the differentiation of therapeutic insulin-producing cells, which formed islet-like cell clusters with extensive capillary networks and regulated blood glucose levels in experimental diabetic mice.[40] Moreover, to improve the diseased organ-targeted efficiency of unmodified ENVs in spinal cord injury (SCI) treatment, whether achieved by fusing macrophage membranes with ENVs for targeted delivery to ischemic and inflamed organs, or by engineering magnet-guided ENVs through iron oxide pretreatment, remarkably enhanced targeting efficiency and the feasibility of promoting functional recovery in the spinal cord were observed in SCI mouse model.[36,65] Besides, magnet-guided ENVs also exhibited promising therapeutic potential in cardiac repair. Lee et al[38] demonstrated that these modified ENVs not only significantly improved their retention in infarcted heart but also facilitated the recovery of cardiac function. Collectively, due to their distinctive structures and properties, ENVs have promising prospects in multiple fields. However, there has been no relevant research on targeted delivery of bioinspired ENVs in the field of atherosclerotic treatment.

Taking inspiration from the aforementioned studies, we found that the administration of ENVs led to a reduction in atherosclerotic plaque area. In comparison to these unmodified ENVs, the administration of P-ENVs further enhanced anti-atherosclerotic efficacy through targeted delivery to atherosclerotic lesions. It is well established that foam cells play a pivotal role in the initiation and progression of atherosclerosis. With the deposition of excessive cholesterol in atherosclerotic lesions, an increase in cholesterol influx and esterification and/or a decrease in cholesterol efflux ultimately lead to foam cell formation.[3] Excessive cholesterol outflow, commonly known as RCT,[66] is pivotal in maintaining cholesterol balance and preventing atherosclerosis.[67] ABCA1, a pivotal regulator of RCT, primarily mediates the transfer of phospholipids and cholesterol across cellular bilayer membranes to lipid-poor APOA-I. This pivotal interaction between ABCA1 and APOA-I catalyzes the nascent formation of HDL particles.[68,69] ABCG1 engages in the RCT process at a subsequent stage, directing cholesterol efflux to mature HDL particles rather than to lipid-poor APOA-I.[70,71] Collectively, these transporters synergize to maintain cellular cholesterol homeostasis and prevent the accumulation of excess cholesterol within the arterial walls. With the advancement in single-cell sequencing technology and lineage tracing, recent studies have unveiled new insights into the origin of foam cells in atherosclerotic lesions. Except for well-known macrophage-derived foam cells, it has been demonstrated that a majority of foam cells originate from VSMCs.[72] Notably, these VSMC-derived foam cells exhibited lower expression levels of ABCA1 compared with macrophage-derived foam cells,[72,73] and the reduced expression of ABCA1 in VSMC-derived foam cells offered a compelling explanation for the observed resistance to regression, which may shed light on VSMCs over macrophages as the primary source of foam cells in atherosclerotic lesions. In our study, after extraction and analysis of total RNA, both the ENV and P-ENV groups exhibited similar numbers of target genes and rich factors in the regulation of intracellular cholesterol metabolism. Through a comprehensive exploration of miRNA-target gene interactions in the cholesterol metabolism signaling pathway, we demonstrated a strong association between miRNAs in both ENV and P-ENV groups and the expression of ABCA1 in the cholesterol metabolism pathway. To further verify the impact of P-ENV treatment on ABCA1 expression in vitro, our studies showed that P-ENV treatment significantly upregulated the expression of

cholesterol transporter-associated protein ABCA1 and ABCG1, concomitant with an increase in cholesterol efflux and a reduction in intracellular total cholesterol content. In line with these findings in vitro, an in vivo study further validated the influence of P-ENVs on the expression of ABCA1 and ABCG1. Collectively, these results indicated that P-ENVs hold promise for potential anti-atherosclerotic treatment by modulating the cholesterol metabolism of foam cells through the regulation of ABCA1 and ABCG1 expression.

There are several limitations in our study. Firstly, although this study has achieved encouraging anti-atherosclerotic effects, similar to other studies in this field,[46,47,74–76] there are concerns regarding the long-term safety and potential side effects associated with the use of nanoparticles in atherosclerotic treatment. Secondly, considering the importance of VSMC-derived foam cells in atherosclerotic development,[72] this study has focused on examining the modulatory impact of ENVs on these cells. Nonetheless, the effects on macrophage-derived foam cells still require further validation. Thirdly, the specific interactions between ENVs and cells within atherosclerotic plaques, and whether the biological membranes affect the entry of vesicles into the recipient cells, need to be further explored. Fourthly, the primary objective of this study is to assess and validate the feasibility and therapeutic potential of targeted delivery via platelet membrane fused ENVs for the treatment of atherosclerosis. There remains a need to elucidate the detailed molecular mechanisms by which these vesicles reverse foam cell formation in future research.

Conclusion

In summary, we have synthetically produced P-ENVs as a novel atherosclerosis-targeted drug delivery system for the treatment of atherosclerosis. Based on the inherent targeting ability of platelets towards atherosclerotic plaques, P-ENVs enhance targeted delivery to atherosclerotic plaques, significantly enhancing the therapeutic efficacy of ENVs while simultaneously minimizing adverse effects. In comparison to traditional exosomes, ENVs emerge as a promising nanotherapeutic agent for atherosclerotic treatment, with a high potential for large-scale production. Our study is the first to apply ENVs in the treatment of atherosclerosis and paves the way for leveraging nanomedicine to develop more effective therapeutic approaches for atherosclerosis. As a crucial component of atherosclerotic treatment strategy, the nanodrug delivery platform holds promising potential for future applications.

Abbreviations

MSCs, Mesenchymal stem cells; P-ENVs, Platelet membrane-coated exosome-mimetic nanovesicles; ENVs, Exosome-mimetic nanovesicles; TEM, Transmission electron microscopy; NTA, Nanoparticle tracking analysis; IVIS, In vivo imaging system; ORO, Oil Red O; EVs, Extracellular vesicles; P-NPs, Platelet membrane-coated nanoparticles; IMDM, Iscove's modified dulbecco's medium; VSMCs, Vascular smooth muscle cells; HSMCs, Human aortic smooth muscle cells; MVSMCs, Mouse aortic vascular smooth muscle cells; DMEM/F-12, Dulbecco's modified eagle medium/nutrient mixture F-12; HUVECs, Human umbilical vein endothelial cells; DMEM, Dulbecco's modified eagle medium; ECM, Endothelial cell medium; PBS, Phosphate buffered saline; EDTA, Ethylene diamine tetraacetic acid; PRP, Platelet rich plasma; PGE1, Prostaglandin E1; PEG, Polyethylene glycol; LPS, Lipopolysaccharide; FBS, Fetal bovine serum; OD, Optical density; GO, Gene ontology; KEGG, Kyoto encyclopedia of genes and genomes; vWF, von Willebrand factor; NBD, Nitrobenzoxadiazolyl; APOA-I, Apolipoprotein A-I; FI, Fluorescence intensity; HE, Hematoxylin-eosin; SD, Standard deviation; RES, Reticuloendothelial system; ICAM-1, Intracellular adhesion molecule-1; TG, Triglyceride; TC; Total cholesterol; LDL, Low-density lipoprotein; HDL, High-density lipoprotein; RBCs, Red blood cells; WBCs, White blood cells; PLTs, Platelets; HGB, Hemoglobin; CREA, Creatinine; BUN, Blood urea nitrogen; ALT, Alanine aminotransferase; AST, Aspartate aminotransferase; DPCs, Dermal papilla cells; SCI, Spinal cord injury; RCT, Reverse cholesterol transport.

Data Sharing Statement

The datasets used and analyzed during the current study are available from the corresponding author.

Ethics Approval and Informed Consent

The animal experiment was conducted under the approval and supervision of the Experimental Animals Ethics Committee of Fuwai Hospital (FW-2022-0027), and all procedures met the National Institutes of Health guidelines. All human experiments were performed in line with the Ethics Committee of Fuwai Hospital (FW-2020-1317) and followed the guidelines outlined in the Declaration of Helsinki. Besides, informed consent was obtained from the study participants.

Consent for Publication

All authors agree to publish this paper in this journal.

Author Contributions

All authors made a significant contribution to the work reported, whether that is in the conception, study design, execution, acquisition of data, analysis and interpretation, or in all these areas; took part in drafting, revising, or critically reviewing the article; gave final approval of the version to be published; have agreed on the journal to which the article has been submitted; and agree to be accountable for all aspects of the work.

Funding

Disclosure

None of the authors declare any conflicts of interest.

References

1. Wang D, Yang Y, Lei Y, et al. Targeting foam cell formation in atherosclerosis: therapeutic potential of natural products. *Pharmacol Rev.* 2019;71(4):596–670. doi:10.1124/pr.118.017178
2. Ouimet M, Barrett TJ, Fisher EA. HDL and reverse cholesterol transport. *Circ Res.* 2019;124(10):1505–1518. doi:10.1161/CIRCRESAHA.119.312617
3. Yu XH, Fu YC, Zhang DW, Yin K, Tang CK. Foam cells in atherosclerosis. *Clin Chim Acta.* 2013;424:245–252. doi:10.1016/j.cca.2013.06.006
4. Zhang J, Zu Y, Dhanasekara CS, et al. Detection and treatment of atherosclerosis using nanoparticles. *Wiley Interdiscip Rev Nanomed Nanobiotechnol.* 2017;9:1.
5. Zi Y, Yang K, He J, Wu Z, Liu J, Zhang W. Strategies to enhance drug delivery to solid tumors by harnessing the EPR effects and alternative targeting mechanisms. *Adv Drug Deliv Rev.* 2022;188:114449. doi:10.1016/j.addr.2022.114449
6. Fang J, Islam W, Maeda H. Exploiting the dynamics of the EPR effect and strategies to improve the therapeutic effects of nanomedicines by using EPR effect enhancers. *Adv Drug Deliv Rev.* 2020;157:142–160. doi:10.1016/j.addr.2020.06.005
7. Pillai SC, Borah A, Le MNT, Kawano H, Hasegawa K, Kumar DS. Co-delivery of curcumin and Bioperine via PLGA nanoparticles to prevent atherosclerotic foam cell formation. *Pharmaceutics.* 2021;13:9.
8. Mu D, Wang X, Wang H, et al. Chemiexcited photodynamic therapy integrated in polymeric nanoparticles capable of MRI against atherosclerosis. *Int J Nanomed.* 2022;17:2353–2366. doi:10.2147/IJN.S355790
9. Esfandyari-Manesh M, Abdi M, Talasaz AH, Ebrahimi SM, Atyabi F, Dinarvand R. S2P peptide-conjugated PLGA-Maleimide-PEG nanoparticles containing Imatinib for targeting drug delivery to atherosclerotic plaques. *Daru.* 2020;28(1):131–138. doi:10.1007/s40199-019-00324-w
10. Gao C, Liu C, Chen Q, et al. Cyclodextrin-mediated conjugation of macrophage and liposomes for treatment of atherosclerosis. *J Control Release.* 2022;349:2–15. doi:10.1016/j.jconrel.2022.06.053
11. Dhanasekara CS, Zhang J, Nie S, Li G, Fan Z, Wang S. Nanoparticles target intimal macrophages in atherosclerotic lesions. *Nanomedicine.* 2021;32:102346. doi:10.1016/j.nano.2020.102346
12. Pham LM, Kim EC, Ou W, et al. Targeting and clearance of senescent foamy macrophages and senescent endothelial cells by antibody-functionalized mesoporous silica nanoparticles for alleviating aorta atherosclerosis. *Biomaterials.* 2021;269:120677. doi:10.1016/j.biomaterials.2021.120677
13. De Jong WH, Borm PJ. Drug delivery and nanoparticles: applications and hazards. *Int J Nanomed.* 2008;3(2):133–149. doi:10.2147/ijn.s596
14. Zhen X, Cheng P, Pu K. Recent Advances in cell membrane-camouflaged nanoparticles for cancer phototherapy. *Small.* 2019;15(1):e1804105. doi:10.1002/smll.201804105
15. Gao M, Liang C, Song X, et al. Erythrocyte-membrane-enveloped perfluorocarbon as nanoscale artificial red blood cells to relieve tumor hypoxia and enhance cancer radiotherapy. *Adv Mater.* 2017;29:35.
16. Wang Y, Zhang K, Qin X, et al. Biomimetic nanotherapies: red blood cell based core-shell structured nanocomplexes for atherosclerosis management. *Adv Sci.* 2019;6(12):1900172. doi:10.1002/advs.201900172

17. Mehta S, Bongcaron V, Nguyen TK, et al. An ultrasound-responsive theranostic cyclodextrin-loaded nanoparticle for multimodal imaging and therapy for atherosclerosis. *Small*. 2022;18(31):e2200967. doi:10.1002/smll.202200967

18. Kim M, Sahu A, Hwang Y, et al. Targeted delivery of anti-inflammatory cytokine by nanocarrier reduces atherosclerosis in Apo E(-/-) mice. *Biomaterials*. 2020;226:119550. doi:10.1016/j.biomaterials.2019.119550

19. Wang C, Zhang Y, Dong Y. Lipid nanoparticle-mRNA formulations for therapeutic applications. *Acc Chem Res*. 2021;54(23):4283–4293. doi:10.1021/acs.accounts.1c00550

20. Goutas D, Pergaris A, Goutas N, Theocharis S. Utilizing exosomal-EPHs/ephrins as biomarkers and as a potential platform for targeted delivery of therapeutic exosomes. *Int J Mol Sci*. 2022;23:7.

21. Brezgin S, Parodi A, Kostyusheva A, et al. Technological aspects of manufacturing and analytical control of biological nanoparticles. *Biotechnol Adv*. 2023;64:108122. doi:10.1016/j.biotechadv.2023.108122

22. Yang W, Yin R, Zhu X, et al. Mesenchymal stem-cell-derived exosomal miR-145 inhibits atherosclerosis by targeting JAM-A. *Mol Ther Nucleic Acids*. 2021;23:119–131. doi:10.1016/j.omtn.2020.10.037

23. Xing X, Li Z, Yang X, et al. Adipose-derived mesenchymal stem cells-derived exosome-mediated microRNA-342-5p protects endothelial cells against atherosclerosis. *Aging*. 2020;12(4):3880–3898. doi:10.18632/aging.102857

24. Zhang N, Luo Y, Zhang H, Zhang F, Gao X, Shao J. Exosomes derived from mesenchymal stem cells ameliorate the progression of Atherosclerosis in ApoE(-/-) Mice via FENDRR. *Cardiovasc Toxicol*. 2022;22(6):528–544. doi:10.1007/s12012-022-09736-8

25. Safari S, Malekvandfard F, Babashah S, Alizadehasl A, Sadeghizadeh M, Motavaf M. Mesenchymal stem cell-derived exosomes: a novel potential therapeutic avenue for cardiac regeneration. *Cell Mol Biol*. 2016;62(7):66–73.

26. Valadi H, Ekstrom K, Bossios A, Sjostrand M, Lee JJ, Lotvall JO. Exosome-mediated transfer of mRNAs and microRNAs is a novel mechanism of genetic exchange between cells. *Nat Cell Biol*. 2007;9(6):654–659. doi:10.1038/ncb1596

27. Pan Y, Wu W, Jiang X, Liu Y. Mesenchymal stem cell-derived exosomes in cardiovascular and cerebrovascular diseases: from mechanisms to therapy. *Biomed Pharmacother*. 2023;163:114817. doi:10.1016/j.biopha.2023.114817

28. Zou D, Yang P, Liu J, et al. Exosome-Loaded Pro-efferocytic Vascular Stent with Lp-PLA(2)-Triggered Release for Preventing In-Stent Restenosis. *ACS Nano*. 2022;16(9):14925–14941. doi:10.1021/acsnano.2c05847

29. Sun L, He X, Zhang T, Han Y, Tao G. Knockdown of mesenchymal stem cell-derived exosomal LOC100129516 suppresses the symptoms of atherosclerosis via upregulation of the PPARgamma/LXRalpha/ABCA1 signaling pathway. *Int J Mol Med*. 2021;48:6.

30. Ma J, Chen L, Zhu X, Li Q, Hu L, Li H. Mesenchymal stem cell-derived exosomal miR-21a-5p promotes M2 macrophage polarization and reduces macrophage infiltration to attenuate atherosclerosis. *Acta Biochim Biophys Sin*. 2021;53(9):1227–1236. doi:10.1093/abbs/gmab102

31. Li J, Xue H, Li T, et al. Exosomes derived from mesenchymal stem cells attenuate the progression of atherosclerosis in ApoE(-/-) mice via miR-let7 mediated infiltration and polarization of M2 macrophage. *Biochem Biophys Res Commun*. 2019;510(4):565–572. doi:10.1016/j.bbrc.2019.02.005

32. Yoon J, Jo W, Jeong D, Kim J, Jeong H, Park J. Generation of nanovesicles with sliced cellular membrane fragments for exogenous material delivery. *Biomaterials*. 2015;59:12–20. doi:10.1016/j.biomaterials.2015.04.028

33. Barile L, Vassalli G. Exosomes: therapy delivery tools and biomarkers of diseases. *Pharmacol Ther*. 2017;174:63–78. doi:10.1016/j.pharmthera.2017.02.020

34. Wiklander OP, Nordin JZ, O'Loughlin A, et al. Extracellular vesicle in vivo biodistribution is determined by cell source, route of administration and targeting. *J Extracell Vesicles*. 2015;4:26316. doi:10.3402/jev.v4.26316

35. Lai CP, Mardini O, Ericsson M, et al. Dynamic biodistribution of extracellular vesicles in vivo using a multimodal imaging reporter. *ACS Nano*. 2014;8(1):483–494. doi:10.1021/nn404945r

36. Lee JR, Kyung JW, Kumar H, et al. Targeted delivery of mesenchymal stem cell-derived nanovesicles for spinal cord injury treatment. *Int J Mol Sci*. 2020;21:11.

37. Cao L, Tian T, Huang Y, et al. Neural progenitor cell-derived nanovesicles promote hair follicle growth via miR-100. *J Nanobiotechnology*. 2021;19(1):20. doi:10.1186/s12951-020-00757-5

38. Lee JR, Park BW, Kim J, et al. Nanovesicles derived from iron oxide nanoparticles-incorporated mesenchymal stem cells for cardiac repair. *Sci Adv*. 2020;6(18):eaaz0952. doi:10.1126/sciadv.aaz0952

39. Jo W, Jeong D, Kim J, Park J. Self-renewal of bone marrow stem cells by nanovesicles engineered from embryonic stem cells. *Adv Healthc Mater*. 2016;5(24):3148–3156. doi:10.1002/adhm.201600810

40. Oh K, Kim SR, Kim DK, et al. In vivo differentiation of therapeutic insulin-producing cells from bone marrow cells via extracellular vesicle-mimetic nanovesicles. *ACS Nano*. 2015;9(12):11718–11727. doi:10.1021/acsnano.5b02997

41. Jo W, Kim J, Yoon J, et al. Large-scale generation of cell-derived nanovesicles. *Nanoscale*. 2014;6(20):12056–12064. doi:10.1039/c4nr02391a

42. Jang SC, Kim OY, Yoon CM, et al. Bioinspired exosome-mimetic nanovesicles for targeted delivery of chemotherapeutics to malignant tumors. *ACS Nano*. 2013;7(9):7698–7710. doi:10.1021/nn402232g

43. Choo YW, Kang M, Kim HY, et al. M1 macrophage-derived nanovesicles potentiate the anticancer efficacy of immune checkpoint inhibitors. *ACS Nano*. 2018;12(9):8977–8993. doi:10.1021/acsnano.8b02446

44. Lee Y, Kim M, Ha J, Lee M. Brain-targeted exosome-mimetic cell membrane nanovesicles with therapeutic oligonucleotides elicit anti-tumor effects in glioblastoma animal models. *Bioeng Transl Med*. 2023;8(2):e10426. doi:10.1002/btm2.10426

45. Modery-Pawlowski CL, Kuo HH, Baldwin WM, Sen Gupta A. A platelet-inspired paradigm for nanomedicine targeted to multiple diseases. *Nanomedicine*. 2013;8(10):1709–1727. doi:10.2217/nnm.13.113

46. Yin M, Lin J, Yang M, et al. Platelet membrane-cloaked selenium/ginsenoside Rb1 nanosystem as biomimetic reactor for atherosclerosis therapy. *Colloids Surf B Biointerfaces*. 2022;214:112464. doi:10.1016/j.colsurfb.2022.112464

47. Song Y, Huang Z, Liu X, et al. Platelet membrane-coated nanoparticle-mediated targeting delivery of Rapamycin blocks atherosclerotic plaque development and stabilizes plaque in apolipoprotein E-deficient (ApoE(-/-)) mice. *Nanomedicine*. 2019;15(1):13–24. doi:10.1016/j.nano.2018.08.002

48. Banskota S, Yousefpour P, Chilkoti A. Cell-based biohybrid drug delivery systems: the best of the synthetic and natural worlds. *Macromol Biosci*. 2017;17:1.

49. Fang RH, Jiang Y, Fang JC, Zhang L. Cell membrane-derived nanomaterials for biomedical applications. *Biomaterials*. 2017;128:69–83. doi:10.1016/j.biomaterials.2017.02.041

50. Luk BT, Zhang L. Cell membrane-camouflaged nanoparticles for drug delivery. *J Control Release*. 2015;220(Pt B):600–607. doi:10.1016/j.jconrel.2015.07.019

51. Klyachko NL, Arzt CJ, Li SM, Gololobova OA, Batrakova EV. Extracellular vesicle-based therapeutics: preclinical and clinical investigations. *Pharmaceutics*. 2020;12:12.

52. Huang HC, Wang TY, Rousseau J, et al. Lesion-specific suppression of YAP/TAZ by biomimetic nanodrug ameliorates atherosclerosis development. *bioRxiv*. 2023. doi:10.1101/2023.04.24.537992

53. Hu CM, Fang RH, Wang KC, et al. Nanoparticle biointerfacing by platelet membrane cloaking. *Nature*. 2015;526(7571):118–121. doi:10.1038/nature15373

54. Dehaini D, Wei X, Fang RH, et al. Erythrocyte-platelet hybrid membrane coating for enhanced nanoparticle functionalization. *Adv Mater*. 2017;29:16.

55. Hu Q, Sun W, Qian C, Wang C, Bomba HN, Gu Z. Anticancer platelet-mimicking nanovehicles. *Adv Mater*. 2015;27(44):7043–7050. doi:10.1002/adma.201503323

56. Simberg D, Duza T, Park JH, et al. Biomimetic amplification of nanoparticle homing to tumors. *Proc Natl Acad Sci U S A*. 2007;104(3):932–936. doi:10.1073/pnas.0610298104

57. Anselmo AC, Modery-Pawlowski CL, Menegatti S, et al. Platelet-like nanoparticles: mimicking shape, flexibility, and surface biology of platelets to target vascular injuries. *ACS Nano*. 2014;8(11):11243–11253. doi:10.1021/nn503732m

58. Wei X, Gao J, Fang RH, et al. Nanoparticles camouflaged in platelet membrane coating as an antibody decoy for the treatment of immune thrombocytopenia. *Biomaterials*. 2016;111:116–123. doi:10.1016/j.biomaterials.2016.10.003

59. Huo Y, Ley KF. Role of platelets in the development of atherosclerosis. *Trends Cardiovasc Med*. 2004;14(1):18–22. doi:10.1016/j.tcm.2003.09.007

60. Gawaz M, Langer H, May AE. Platelets in inflammation and atherogenesis. *J Clin Invest*. 2005;115(12):3378–3384. doi:10.1172/JCI27196

61. Chen J, Lopez JA. Interactions of platelets with subendothelium and endothelium. *Microcirculation*. 2005;12(3):235–246. doi:10.1080/10739680590925484

62. Badimon L, Vilahur G. Thrombosis formation on atherosclerotic lesions and plaque rupture. *J Intern Med*. 2014;276(6):618–632. doi:10.1111/joim.12296

63. Armstrong PC, Kirkby NS, Chan MV, et al. Novel whole blood assay for phenotyping platelet reactivity in mice identifies ICAM-1 as a mediator of platelet-monocyte interaction. *Blood*. 2015;126(10):e11–8. doi:10.1182/blood-2015-01-621656

64. Coenen DM, Mastenbroek TG, Cosemans J. Platelet interaction with activated endothelium: mechanistic insights from microfluidics. *Blood*. 2017;130(26):2819–2828. doi:10.1182/blood-2017-04-780825

65. Kim HY, Kumar H, Jo MJ, et al. Therapeutic Efficacy-potentiated and diseased organ-targeting nanovesicles derived from mesenchymal stem cells for spinal cord injury treatment. *Nano Lett*. 2018;18(8):4965–4975. doi:10.1021/acs.nanolett.8b01816

66. Rosenson RS, Brewer HB, Davidson WS, et al. Cholesterol efflux and atheroprotection: advancing the concept of reverse cholesterol transport. *Circulation*. 2012;125(15):1905–1919. doi:10.1161/CIRCULATIONAHA.111.066589

67. Li G, Gu HM, Zhang DW. ATP-binding cassette transporters and cholesterol translocation. *IUBMB Life*. 2013;65(6):505–512. doi:10.1002/iub.1165

68. Singaraja RR, Van Eck M, Bissada N, et al. Both hepatic and extrahepatic ABCA1 have discrete and essential functions in the maintenance of plasma high-density lipoprotein cholesterol levels in vivo. *Circulation*. 2006;114(12):1301–1309. doi:10.1161/CIRCULATIONAHA.106.621433

69. Singaraja RR, Fievet C, Castro G, et al. Increased ABCA1 activity protects against atherosclerosis. *J Clin Invest*. 2002;110(1):35–42. doi:10.1172/JCI15748

70. Wang N, Lan D, Chen W, Matsuura F, Tall AR. ATP-binding cassette transporters G1 and G4 mediate cellular cholesterol efflux to high-density lipoproteins. *Proc Natl Acad Sci U S A*. 2004;101(26):9774–9779. doi:10.1073/pnas.0403506101

71. Vaughan AM, Oram JF. ABCG1 redistributes cell cholesterol to domains removable by high density lipoprotein but not by lipid-depleted apolipoproteins. *J Biol Chem*. 2005;280(34):30150–30157. doi:10.1074/jbc.M505368200

72. Wang Y, Dubland JA, Allahverdian S, et al. Smooth muscle cells contribute the majority of foam cells in ApoE (Apolipoprotein E)-deficient mouse atherosclerosis. *Arterioscler Thromb Vasc Biol*. 2019;39(5):876–887. doi:10.1161/ATVBAHA.119.312434

73. Allahverdian S, Chehroudi AC, McManus BM, Abraham T, Francis GA. Contribution of intimal smooth muscle cells to cholesterol accumulation and macrophage-like cells in human atherosclerosis. *Circulation*. 2014;129(15):1551–1559. doi:10.1161/CIRCULATIONAHA.113.005015

74. Ma Y, Ma Y, Gao M, et al. Platelet-mimicking therapeutic system for noninvasive mitigation of the progression of atherosclerotic plaques. *Adv Sci*. 2021;8(8):2004128. doi:10.1002/advs.202004128

75. Chen L, Zhou Z, Hu C, et al. Platelet membrane-coated nanocarriers targeting plaques to deliver anti-CD47 antibody for atherosclerotic therapy. *Research*. 2022;2022:9845459. doi:10.34133/2022/9845459

76. Wu G, Zhang J, Zhao Q, et al. Molecularly engineered macrophage-derived exosomes with inflammation tropism and intrinsic heme biosynthesis for atherosclerosis treatment. *Angew Chem Int Ed Engl*. 2020;59(10):4068–4074. doi:10.1002/anie.201913700